Development of an Attitude Control System For a Large Scale Multicopter VTOL Aircraft

Rustom F. Jehangir
rjehangir@advancedtacticsinc.com
Chief Engineer
Advanced Tactics Inc.
El Segundo, California, USA

ABSTRACT

Multicopter type helicopters have become prevalent in the past ten years with applications in military, academia, commercial, and recreational use. These aircraft benefit from their inherent simplicity, robust design, and ease of control. This paper discusses the design of an attitude control system for a large-scale gas powered multicopter and the challenges overcome in the development of the system. A nonlinear model was developed for simulation purposes and a simplified linear model was developed for control system design. The resulting control system architecture and design was implemented and successfully tested on an eight-engine prototype aircraft with 880 horsepower and a max gross weight of 4,400 lb.

NOTATION

C_P	propeller coefficient of power
C_Q	propeller coefficient of torque
C_T	propeller coefficient of thrust
D	propeller diameter, ft
F_{A_i}	aerodynamic force along axis, i, lb
F_{T_i}	thrust force along axis, i, lb
h	height above reference point, ft
$\mathbf{I}$	moment of inertia tensor matrix
L	rolling moment, ft-lb
L_A	aerodynamic moment about **x**-axis, ft-lb
L_T	thrust moment about **x**-axis, ft-lb
m	aircraft mass, slugs
M	pitching moment, ft-lb
M_A	aerodynamic moment about **y**-axis, ft-lb
M_T	thrust moment about **y**-axis, ft-lb
N_A	aerodynamic moment about **z**-axis, ft-lb
N_T	thrust moment about **z**-axis, ft-lb
n	propeller rotational speed, rev/sec
N	yawing moment, ft-lb
N_{ENGINES}	number of engines and propellers
P	roll rate, rad/s
P_N	position north of reference point, ft
P_E	position east of reference point, ft
Q	pitch rate, rad/s
Q	propeller torque, ft-lb
R	yaw rate, rad/s
T	propeller thrust, lb
T_n	propeller thrust due to rotational speed, lb
$T_{\dot{\phi}}$	propeller thrust due to rolling rate, lb
$T_{\dot{\theta}}$	propeller thrust due to pitching rate, lb
u	input to control system
U	velocity in the **x**-axis, ft/s
V	velocity in the **y**-axis, ft/s
V_{TIP}	propeller tip speed, ft/s
W	velocity in the **z**-axis, ft/s
x_{ARM}	propeller moment arm from CG, ft
x_{YAW}	moment arm from CG of tilted propeller for yaw, ft
y_{ARM}	propeller moment arm from CG, ft
θ	pitch angle, deg
ρ	air density, slugs/ft^3
ϕ	roll angle, deg
ϕ_{YAW}	engine tilt angle for yaw, deg
ψ	yaw angle (heading), deg

Presented at the AHS 70th Annual Forum, Montréal, Québec, Canada, May 20–22, 2014.

INTRODUCTION

The *Advanced Tactics' Black Knight Transformer (BKT)* (patented and patent pending) is a roadable multi-engine vertical takeoff and landing (VTOL) aircraft designed for casualty evacuation and cargo resupply operations. The aircraft's design was motivated primarily by a set of unique operational requirements and the need for a simple, low-cost design. The aircraft is required to be roadable, meaning that it has a ground driving system and is designed to fit within the size limitations of an automobile. It is also required to achieve VTOL flight with a reasonable payload lifting capacity. To satisfy these requirements, a multicopter design was chosen because it produces a compact vehicle with minimal mechanical complexity. Like electric multicopters, the aircraft uses fixed pitch propellers that are directly driven by individual engines, reducing the system cost by eliminating the mechanisms needed for collective and cyclic pitch control used in conventional rotorcraft. This paper presents the challenges associated with such a system, a method of modeling the aircraft's dynamics, and the control system architecture and design used for the prototype demonstrator aircraft.

History

To date, there have been a number of large scale multicopter aircraft that have flown. Early attempts were made by Oehmichen and de Bothezat in the early 1920s. In the 1950s and 1960s, several more attempts were made including the Convertawing Model A Quadrotor, the Curtiss-Wright VZ-7, and the Curtiss-Wright X-19. These aircraft are shown in Fig. 1. They were all stabilized and controlled with variable thrust controlled by the collective pitch of each rotor and all performed successful tests but they were difficult to handle and stabilize.

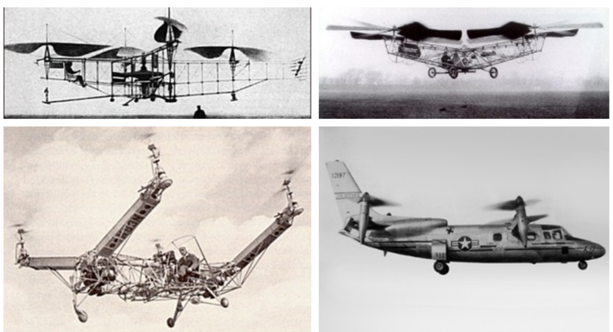

Fig. 1: The 1921 Oehmichen quadrotor (top left), the 1923 de Bothezat Quadrotor (top right), the 1956 Convertawing Model A Quadrotor (bottom left), and the 1963 Curtiss-Wright X-19 (bottom right).

The use of collective rotor pitch control provides a high-bandwidth control effector, however the mechanisms required to implement such a solution add complexity and cost to the aircraft. In recent years, the advent of low-cost microelectronics and sensors has spurred the development of many small electric multicopters. With a few exceptions, these aircraft are controlled with variations in propeller speed instead of propeller pitch to vary thrust. This provides a simple, elegant, and low-cost design with few moving parts. An example of such an aircraft is shown in Fig. 2.

Fig. 2: A commercial electric quadcopter.

The Black Knight Transformer

A complete description and justification of the BKT design is beyond the scope of this paper, but an overview will be provided as the context for the modeling and control system design. The aircraft is a multicopter, using eight vertically oriented engines and propellers mounted along either side of a central fuselage as shown in Fig. 3. The engines and propellers are mounted to engine arms that extend from the fuselage, which is a simple rectangular design that minimizes weight and maximizes strength. The fuselage has doors on each end and both sides for access to the payload compartment. Because the engines are mounted externally, the interior of the fuselage is mostly open space for cargo or equipment.

The automotive drivetrain utilizes a conventional double wishbone suspension, shocks, brakes, and a separate gas engine and transaxle. The rear wheels are powered and the front wheels steer, similar to a conventional automobile. The steering, braking, and control of the engine and transmission is performed with electric actuators so that the vehicle may be driven remotely. The vehicle is capable of driving at up to 60 mph on the road and has almost two feet of ground clearance for off-road driving. The suspension also provides a cushion for landing, allowing the vehicle to land hard without damage.

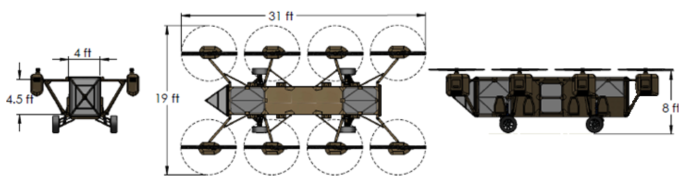

Fig. 3: The prototype demonstrator aircraft configuration.

The BKT uses reciprocating gas engines that are directly driven to fixed pitch propellers through a reduction drive, maintaining the simplicity and low cost that is achieved in the design of small electric multicopters. Unlike any other large scale multicopter in history, the BKT aircraft is controlled with variations in propeller rotational speed to vary the center of thrust. There is no transmission, swash-plate, blade articulation, tail-rotor, control linkages, or any of the complex mechanical systems typical to a helicopter. Table 1 shows the basic specifications of the Black Knight Transformer prototype demonstrator aircraft.

Table 1: Black Knight Transformer Characteristics.

Characteristic	English	Metric
Engines	8 x two-cycle fuel-injected gas	
Engine Power	8 x 110 hp	8 x 82 kW
Width	19 ft	5.8 m
Length	31 ft	9.5 m
Height	8 ft	2.5 m
Propeller Diameter	7 ft	2.13 m
Max Gross Weight	4,400 lb	1,995 kg

The Black Knight Transformer aircraft design is simple and inexpensive. It offers new capabilities and may provide a low-cost platform for future unmanned vertical lift missions such as casualty evacuation and cargo resupply.

CHALLENGES OF A LARGE SCALE MULTICOPTER

The modeling and control system design of multicopter aircraft is a well-known and thoroughly addressed topic. See (Ref. 1), (Ref. 2), and (Ref. 3) for examples of multicopter attitude control system development. However, there are several new challenges to face with a large scale gas powered configuration. These include a slow and nonlinear engine response, limited yaw performance, and engine-out flight performance.

Engine Nonlinearity and Response Time

The biggest difference between a small electric multicopter and the Black Knight Transformer is the use of reciprocating internal combustion (IC) engines. The brushless electric motors used on small multicopters provide high torque to change RPM rapidly, and in many multicopter control analyses they are assumed to have instantaneous responses. IC engines, on the other hand have slow response times and nonlinear response characteristics.

Initial engine testing revealed a number of issues to overcome. First, although the throttle position was calibrated with an empirical mapping, variations in engine temperature and atmospheric conditions produced steady state error. Next, the engine frequency response was identified throughout the RPM range of the engine and was found to vary with respect to RPM. It was also found that torque output limitations of the engine limit the degree to which the engine response can be improved with feedback. Nevertheless, a well-performing controller was developed and provides precise response characteristics that were used to design the flight control systems.

Yaw Control Authority

The second challenge faced is the yaw performance of the aircraft. Typical multicopters use differential rotational speed, and thus torque, between sets of counter rotating propellers to produce a yawing moment. The torque produced by each propeller, Q, can be approximated by

$$Q = C_Q \rho n^2 D^5 \tag{1}$$

where C_Q is the coefficient of torque of the propeller (Ref. 4). To produce a positive yawing moment with the differential torque method, the clockwise (when viewed from above) engine rotational speeds are changed by $-\Delta n$ and the counterclockwise engine rotational speeds are changed by Δn. The sum of propeller torques, $\sum Q_i = Q_{\text{TOTAL}}$, is equivalent to the yawing moment of the aircraft, N, when external forces are ignored.

The lack of yaw control power at a large scale can be illustrated by showing how the propeller torque, Q, and moment of inertia about the **z**-axis, I_{zz}, change as an aircraft is scaled in size. First, the yaw angular acceleration of the aircraft is given by

$$\ddot{\psi} = \frac{N}{I_{zz}}. \tag{2}$$

For the sake of the argument, the aircraft is scaled with a constant propeller coefficient of torque and constant tip speed, V_{TIP}, so that the propeller torque can be calculated from Eq. 1 as

$$Q = C_Q \rho \left(\frac{V_{\text{TIP}}}{\pi D}\right)^2 D^5 = C_Q \rho \left(\frac{V_{\text{TIP}}}{\pi}\right)^2 D^3. \tag{3}$$

The moment of inertia of the aircraft, I_{zz}, can be calculated from

$$I_{zz} = \sum m r^2. \tag{4}$$

As the aircraft is scaled equally in all dimensions, the aircraft's mass increases proportionally to the length cubed,

$$m \propto l^3. \tag{5}$$

Then we can see from Eqn. 4 that the moment of inertia is proportional to length to the fifth power, as

$$I_{zz} \propto l^5. \tag{6}$$

On the other hand, the propeller torque and yawing moment from Eqn. 3 is proportional to length cubed,

$$Q \propto N \propto l^3. \tag{7}$$

Therefore, as the scale increases, Eq. 2 shows that for a given input, the ratio of yawing moment to moment of inertia, i.e. yaw angular acceleration, is proportional to the inverse square of the length.

$$\ddot{\psi} \propto \frac{1}{l^2} \tag{8}$$

In short, as the size of the multicopter increases, it has less and less yaw control power. This applies regardless of the propulsion source. The top plot in Fig. 4 shows the yaw angular acceleration, $\ddot{\psi}$, versus the difference between clockwise and counterclockwise engine speeds, Δn, for the Black Knight Transformer.

To counter this problem, the BKT aircraft was designed with actuators that allow the frontmost and rearmost engines to be tilted ± 5 degrees to allow direct generation of a yawing moment. This patented method provides substantially more yaw control authority and has a neglible effect on the lifting capability of the aircraft. The actuators add complexity to the overall system but provide yaw performance similar to a conventional helicopter. The resulting control authority is shown in the lower plot of Fig. 4 as yaw angular acceleration versus propeller tilt angle. The moment arm of the tilted propellers is shown in Fig. 5.

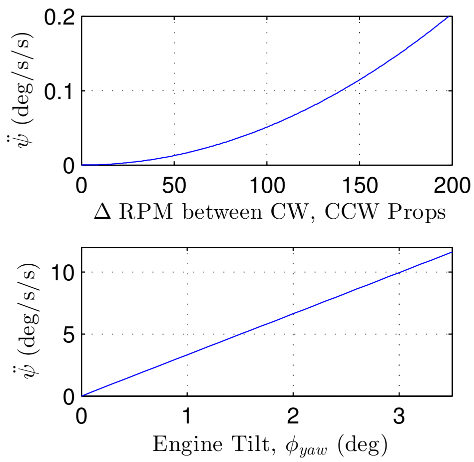

Fig. 4: Comparison of the available yaw control force (shown by aircraft angular acceleration) for the conventional differential torque method versus the yaw tilt actuator method.

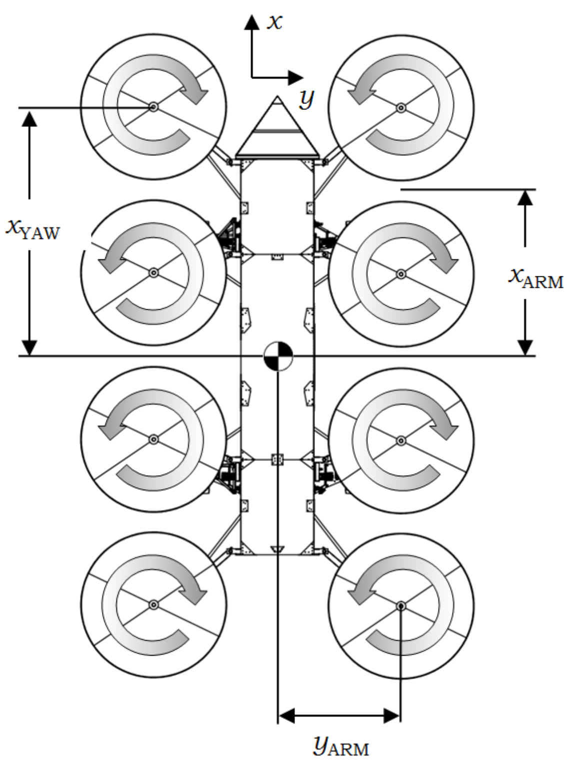

Fig. 5: Diagram of moment arms and propeller rotation directions.

Engine Failures

Reciprocating engines are more prone to failure than the electric motors used on small scale multicopters. Therefore, the ability to handle an engine-out failure is significantly more important. The BKT aircraft was designed to allow for graceful handling of engine failures. The aircraft can continue to maintain complete attitude and yaw control with a failed engine. Fig. 5 shows the rotation directions of the propellers viewed from the top down. If an engine fails, the diagonally opposite engine, which is always spinning in the opposite direction, is shutdown as well. This allows the center of thrust to be maintained at the center of gravity while maintaining an overall torque balance. The yaw actuators continue to provide yaw control.

CONTROL SYSTEM ARCHITECTURE

The electronic control system architecture was designed to allow the control system to be easily implemented with a minimal amount of wiring between electrical systems on the aircraft. An engine control unit (ECU) was developed to interface with each engine and to implement the feedback control of the engine. The control unit uses actuators to adjust the engine throttle position and thereby control the engine speed. A pulse tachometer allows the engine speed to be read at a speed much greater than the attitude control loops. Similarly, an actuator control unit (ACU) was developed to control the actuators that allow the engines to tilt for yaw control. Both units communicate with a central flight control computer through a CAN bus interface. The CAN bus interface, which was developed for use on automobiles, provides a robust digital communication network ideal for control system applications. The arrangement of devices on this network is shown in Fig. 6.

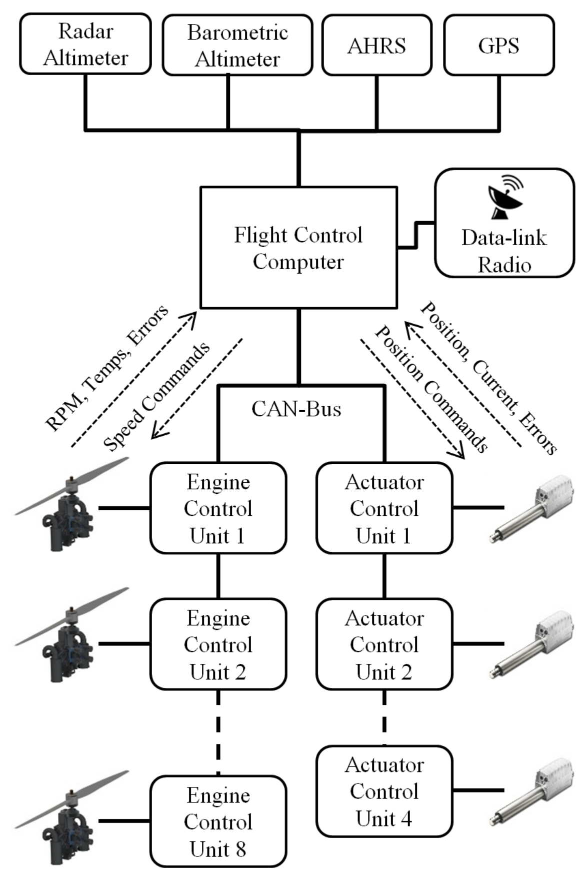

Fig. 6: Architectural arrangement of control system components including engine control units, actuator control units, a flight control computer, and a number of sensors.

In addition to the engine and actuator control units, a number of sensors including an attitude heading reference system

(AHRS), a global positioning system (GPS), radar altimeter, and barometric altimeter. It is also connected to the drivetrain engine, transmission, steering, and brakes through the CAN bus network. The available processing power allows the flight control loop to operate significantly faster than the dynamics of the aircraft so that the discretization of the control system does not significantly affect its performance.

ENGINE MODEL AND RESULTS

Engine Dynamics

Fast and accurate control of the engine/propeller system was the first control system design challenge. Producing a robust engine/propeller system that could be accurately modeled is critical to the higher level control system design. The engine system was first linearized by creating a mapping between the throttle input and the rotational speed output. The mapping was determined empirically. The system response was then identified using frequency domain techniques. An exponential sine sweep input was provided to the engine and the response measured. Matching a linear system to the frequency response provides a second order transfer function for the system that is valid within the rotational speeds used during flight.

A PID controller was applied to the system to increase bandwidth and reduce steady state error. The resulting system has an increase in bandwidth and eliminates steady state error caused by slight variations in engine performance. The added bandwidth helps to stabilize and control the aircraft. The engine's closed loop step response is shown in Fig. 7 and the frequency response is shown in Fig. 8.

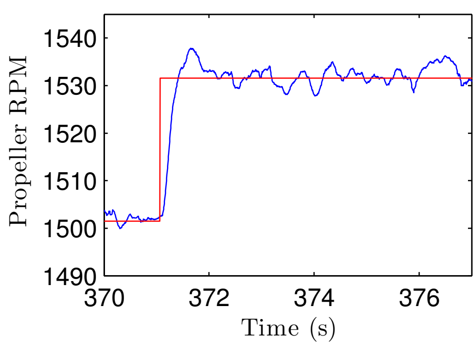

Fig. 7: Typical closed loop step response of the reciprocating engine/propeller system.

SYSTEM MODEL

The following sections develop mathematical models of the important components of the aircraft system. The model is developed under the assumption that the aircraft is in hover conditions or very low speed maneuvering flight. The dynamics of high speed flight are more complicated and are not addressed here. Additionally, only elements of the model needed to design the attitude and attitude rate control systems are presented.

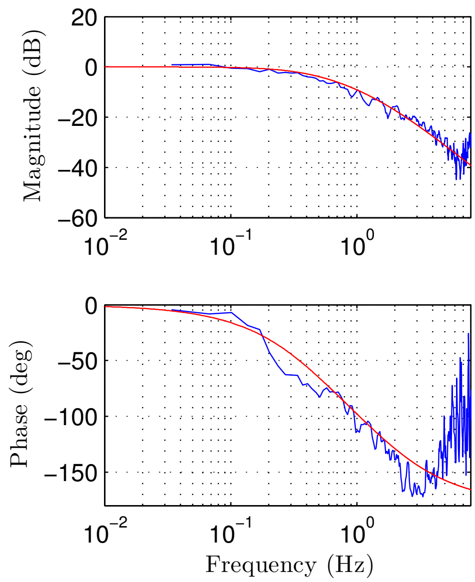

Fig. 8: Frequency response of the closed loop engine system. The red line represents the second order model fitted to the response for controller design.

Axis Systems

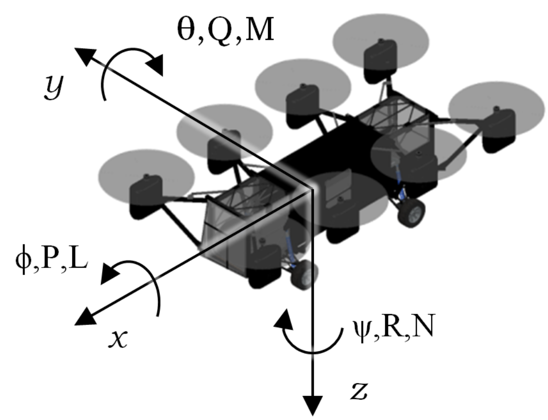

Fig. 9: Axis system diagram used in the development of the aircraft model.

The axis system used for analysis is shown in Fig. 9.

Propeller and Actuator Dynamics

The output of each propeller is considered in two parts: the thrust due to the rotational speed of the propeller, T_n, and the thrust due to rolling and pitching rate, $T_{\dot{\phi}}$ and $T_{\dot{\theta}}$. The second term is caused by variations to the inflow speed caused by rolling and pitching rate. For instance, when the aircraft rolls right, the propellers on the right side of the aircraft experience a decrease in inflow velocity, producing a damping moment. A similar analysis of this effect can be seen in (Ref. 1).

First, the thrust due to the rotational speed of the propeller can be found with

$$T_n = C_T \rho n^2 D^4 \tag{9}$$

from (Ref. 4).

The thrust due to rolling and pitching rate is calculated based on the advance ratio, J, and the coefficient of thrust due to advance ratio, C_{T_J}, as

$$T_{\dot{\phi}} = C_{T_J} J \rho n^2 D^4 \tag{10}$$

J can be calculated as

$$J = \frac{V}{nD} \tag{11}$$

where V is the axial speed of the propeller through the airflow. In static conditions, such as unperturbed hover, J is zero. We calculate the value of V from the angular rate as

$$V_{\text{ROLL}} = y_{\text{ARM}} \dot{\phi} \tag{12}$$

and

$$V_{\text{PITCH}} = x_{\text{ARM}} \dot{\theta}. \tag{13}$$

C_{T_J} is found from empirical data from our engine/propeller system as well as correlated results from other propeller studies. The value of $T_{\dot{\phi}}$ is then calculated with

$$T_{\dot{\phi}} = C_{T_J} \frac{y_{\text{ARM}} \dot{\phi}}{nD} \rho n^2 D^4 = C_{T_J} \rho n D^3 y_{\text{ARM}} \dot{\phi} \tag{14}$$

The value of $T_{\dot{\theta}}$ is similarly found as

$$T_{\dot{\theta}} = C_{T_J} \rho n D^3 x_{\text{ARM}} \dot{\theta}. \tag{15}$$

Combining both thrust terms as well as the moment term from Eqn. 1, the moment generated around each axis by each propeller disc can be found with

$$\begin{pmatrix} M_x \\ M_y \\ M_z \end{pmatrix} = \begin{pmatrix} -C_T \rho n^2 D^4 y_{\text{ARM}} + C_{T_J} \rho n D^3 y_{\text{ARM}}^2 \dot{\phi} \\ C_T \rho n^2 D^4 x_{\text{ARM}} + C_{T_J} \rho n D^3 x_{\text{ARM}}^2 \dot{\theta} \\ C_Q \rho n^2 D^5 \end{pmatrix} \tag{16}$$

The yaw actuators tilt the engines at each end of the aircraft in opposing directions so that the resultant force only acts about the **z**-axis. The tilt angle is given by ϕ_{YAW} and the moment arm is given by x_{YAW}, shown in Fig. 5. Using the small angle approximation, the yaw moment generated by the actuated tilt of the four tilting engines can be calculated as

$$M_z = 4T \phi_{\text{YAW}} x_{\text{YAW}} \tag{17}$$

The resulting forces and moments from the propellers can be calculated with

$$\begin{pmatrix} F_{T_x} \\ F_{T_y} \\ F_{T_z} \end{pmatrix} = \begin{pmatrix} 0 \\ 0 \\ \sum_{i=1}^{8} C_T \rho n_i^2 D^4 \end{pmatrix} \tag{18}$$

and

$$\begin{pmatrix} L_T \\ M_T \\ N_T \end{pmatrix} = \begin{pmatrix} \sum_{i=1}^{8} [-C_T \rho n_i^2 D^4 y_{\text{ARM}} + C_{T_J} \rho n_i D^3 y_{\text{ARM}}^2 \dot{\phi}] \\ \sum_{i=1}^{8} [C_T \rho n_i^2 D^4 x_{\text{ARM}} + C_{T_J} \rho n_i D^3 x_{\text{ARM}}^2 \dot{\theta}] \\ \sum_{i=1}^{8} C_Q \rho n_i^3 D^5 + \sum_{i=1}^{4} C_T \rho n_i^2 D^4 \phi_{\text{YAW}} x_{\text{YAW}} \end{pmatrix} \tag{19}$$

Aerodynamic Forces and Moments

The control system design discussed here only applies to the aircraft in hover conditions or at low velocities. The aerodynamic forces and moments are ignored for the purposes of control system design, however they are included in flight simulations. The aerodynamic forces and moments can be calculated with simple approximations. The aerodynamic drag is calculated as a function of equivalent flat plate area, f, which is the area of a flat plate ($C_D = 1$) to produce equal drag to the aircraft (Ref. 5). The values of equivalent flat plate area were found by performing computational fluid dynamics (CFD) estimates of drag at several low speeds. The drag is then estimated as

$$D = \frac{1}{2} \rho f V^2. \tag{20}$$

The aerodynamic moments are assumed to be negligible because the aircraft does not have any wing or tail surfaces and little surface area with sufficient moment arm to produce a significant aerodynamic moment. Therefore the total aerodynamic forces and moments can be calculated with

$$\begin{pmatrix} F_{A_x} \\ F_{A_y} \\ F_{A_z} \end{pmatrix} = \frac{1}{2} \rho \begin{pmatrix} f_x U^2 \\ f_y V^2 \\ f_z W^2 \end{pmatrix} \tag{21}$$

and

$$\begin{pmatrix} L_A \\ M_A \\ N_A \end{pmatrix} = \begin{pmatrix} 0 \\ 0 \\ 0 \end{pmatrix} \tag{22}$$

Equations of Motion

The equations of motion are written under the assumption that the aircraft is a rigid body, that it has constant mass, and that it has bilateral symmetry (Ref. 6). The equations include aerodynamic and propulsion forces and moments that are calculated using the methods described above.

$$\dot{P} = \frac{1}{I_{xx}}[L_A + L_T - QR(I_{zz} - I_{yy}) + (\dot{R} + PQ)I_{xz}] \tag{23}$$

$$\dot{Q} = \frac{1}{I_{yy}}[M_A + M_T + PR(I_{zz} - I_{xx}) - (P^2 + R^2)I_{xz}] \tag{24}$$

$$\dot{R} = \frac{1}{I_{zz}}[N_A + N_T - PR(I_{yy} - I_{xx}) + (QR + \dot{P})I_{xz}] \tag{25}$$

$$\dot{\phi} = P + tan(\theta)(Qsin(\phi) + Rcos(\phi)) \tag{26}$$

$$\dot{\theta} = Qcos(\phi) - Rsin(\phi) \tag{27}$$

$$\dot{\psi} = \frac{1}{cos(\theta)}(Qsin(\phi) + Rcos(\phi)) \tag{28}$$

$$\dot{U} = -gsin(\theta) + RV - QW + \frac{1}{m}(F_{A_x} + F_{T_x}) \tag{29}$$

$$\dot{V} = gsin(\phi)cos(\theta) + PW - RU + \frac{1}{m}(F_{A_y} + F_{T_y}) \tag{30}$$

$$\dot{W} = gcos(\phi)cos(\theta) + QU - PV + \frac{1}{m}(F_{A_z} + F_{T_z}) \tag{31}$$

$$\begin{aligned}\dot{P}_N = {} & Ucos(\theta)cos(\psi) + V[-cos(\phi)sin(\psi) + sin(\phi)sin(\theta)cos(\psi)] \\ & + W[sin(\phi)sin(\psi) + cos(\phi)sin(\theta)cos(\psi)\end{aligned} \tag{32}$$

$$\begin{aligned}\dot{P}_E = {} & Ucos(\theta)sin(\psi) + V[cos(\phi)cos(\psi) + sin(\phi)sin(\theta)sin(\psi)] \\ & + W[-sin(\phi)cos(\psi)cos(\phi)sin(\theta)sin(\psi)]\end{aligned} \tag{33}$$

$$\dot{h} = Usin(\theta) - Vsin(\phi)cos(\theta) - Wcos(\phi)cos(\theta) \tag{34}$$

These equations were used for nonlinear simulation of the aircraft control systems but were not used for control system design. They are presented here for reference.

CONTROLLER DESIGN

The aircraft dynamic model developed previously is linearized around the hover condition for the purposes of control system design.

Simplified Dynamics

The equations of motion were simplified to single-input single-output (SISO) systems suitable for linear control system design approaches. First, the moments about each axis are linearized around the hover condition. The thrust due to rotational speed, T_n, can be written as

$$T_n(t) = 2C_T\rho n_{\text{HOVER}}D^4 n_P(t) + T_{\text{HOVER}} \tag{35}$$

where $n_P(t)$ is the response of the engine due to roll rate input and the thrust is linearized around the hover condition. Similarly, the thrust due to roll rate, $T_{\dot{\phi}}$ can be written as

$$T_{\dot{\phi}}(t) = C_{T_J}\rho n_{\text{HOVER}}D^3 y_{\text{ARM}}\dot{\phi}(t) \tag{36}$$

Knowing that each engine contributes to the rolling moment equally and the moments generated by T_{HOVER} sum to zero, the total rolling moment of the aircraft can be written as

$$\begin{aligned}L(t) = I_{xx}\ddot{\phi}(t) = {} & 2N_{\text{ENGINES}}C_T\rho n_{\text{HOVER}}D^4 y_{\text{ARM}} n_P(t) + \\ & N_{\text{ENGINES}}C_{T_J}\rho n_{\text{HOVER}}D^3 y_{\text{ARM}}^2\dot{\phi}(t)\end{aligned} \tag{37}$$

After performing a Laplace transformation, the transfer function between roll rate and engine speed can be written as

$$\frac{\dot{\phi}(s)}{n_P(s)} = \frac{2N_{\text{ENGINES}}C_T\rho n_{\text{HOVER}}D^4 y_{\text{ARM}}}{I_{xx}s - N_{\text{ENGINES}}C_{T_J}\rho n_{\text{HOVER}}D^3 y_{\text{ARM}}^2}. \tag{38}$$

Similarly, the transfer function between engine response due to pitch rate input, $n_Q(s)$, and pitching rate, $\dot{\theta}(s)$, can be found as

$$\frac{\dot{\theta}(s)}{n_Q(s)} = \frac{2N_{\text{ENGINES}}C_T\rho n_{\text{HOVER}}D^4 x_{\text{ARM}}}{I_{yy}s - N_{\text{ENGINES}}C_{T_J}\rho n_{\text{HOVER}}D^3 x_{\text{ARM}}^2}. \tag{39}$$

These systems can be related to the controller input to the system, $u(s)$, through the engine closed loop transfer function.

$$\frac{n_P(s)}{u_P(s)} = \frac{n_Q(s)}{u_Q(s)} = \text{ENGINE CLTF} \tag{40}$$

The yaw rate system is simpler because there is only one term in the yawing moment equation. From Eqn. 17 we see that

$$I_{zz}\ddot{\psi}(t) = 4T_{\text{HOVER}}x_{\text{YAW}}\phi_{\text{YAW}}(t). \tag{41}$$

After a Laplace transformation, we find the transfer function between the response of the yaw actuator, $\phi_{\text{YAW}}(s)$, and the yaw rate, $\dot{\psi}(s)$.

$$\frac{\dot{\psi}(s)}{\phi_{\text{YAW}}(s)} = \frac{4T_{\text{HOVER}}x_{\text{YAW}}}{sI_{zz}} \tag{42}$$

This system can be related to the controller input, $u(t)$, through the yaw actuator closed loop transfer function,

$$\frac{\phi_{\text{YAW}}(s)}{u_R(s)} = \text{YAW ACTUATOR CLTF} \tag{43}$$

Eqns. 38, 39, and 42 are the roll rate, pitch rate, and yaw rate plants, respectively. Remember that these systems are modeled around the hover conditions and are valid for small inputs.

Control System Design

The aircraft's attitude and rate control systems were developed using the simplified model developed above with common linear control system design approaches. The basic configuration of the control loops is shown in Fig. 10. For the attitude rate, a proportional-integral-derivative (PID) controller with attitude rate feedback is used to provide a suitable response. The integral term allows the controller to compensate for steady-state rate error caused by CG imbalance. The attitude is then controlled by a proportional (P) controller with attitude error feedback. For yaw a proportional-derivative (PD) controller feeding into a lead compensator was used. The lead compensator is required to prevent oscillations due to the slow response of the yaw actuators. Notice that the pilot input controls the desired roll and pitch attitude and the desired yaw

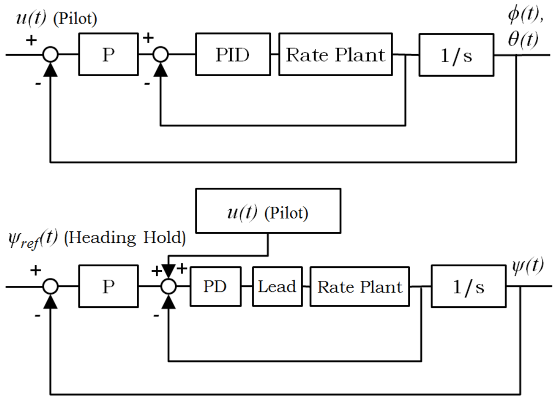

Fig. 10: Control loops for roll, pitch, and yaw rate and attitude control.

rate. With no pilot input the aircraft holds a specified heading that is reset after any pilot input.

A higher-level flight control system for position holding and waypoint navigation has also been developed. This system utilizes the GPS and altimeter, along with a series of waypoints, to provide computer generated inputs to the attitude and heading control systems. Similarly, a third-party higher-level autonomous navigation system could be integrated with the low-level attitude controllers for fully autonomous flight capabilities.

Fig. 11 shows the simulated response of the aircraft to step inputs in roll, pitch, and yaw. As the aircraft is designed for missions such as cargo resupply and casualty evacuation, it was designed with responses similar to those for cargo helicopters. The ADS-33e specification was used to determine required response characteristics in hover (Ref. 7).

CONTROL RESPONSE IN HOVER

As of the writing of this paper, the Black Knight Transformer had recently completed its first flight test. Data was collected during that flight and it is presented here. The flight test was performed near sea level in Southern California. The aircraft was attached to a "kill switch" tether that allowed it to be manually shut down at any point. All flights were short hover flights at an altitude of approximately 5 ft AGL. Fig. 12 shows an image of the aircraft in hover flight.

Figs. 13 and 14 show the attitude of the aircraft during the hover flights. Note that since the aircraft was flown near the ground, there were many disturbance inputs from ground turbulence. The pilot inputs were maintained near zero during the flights and the disturbances were rejected by the attitude control system. Although it has not yet been tested, it is expected that the attitude response of the aircraft will improve further when flown at higher altitudes due to the reduction in disturbance input from ground turbulence.

During several of the test flights, including that shown in Fig. 13, the wind reached approximately 5 knots and was generally aligned with the **x**-axis of the aircraft, causing its position to drift despite a level attitude. Small pilot inputs were made to correct the drift and can be seen in the attitude response of the aircraft. It can be seen that the aircraft was held at a slight nose down attitude to prevent drift.

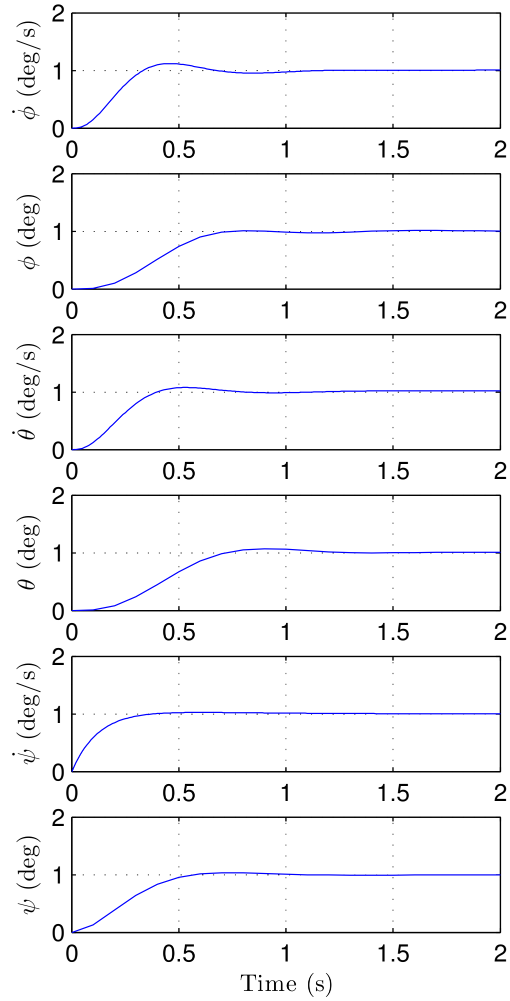

Fig. 11: Simulated step response to roll, pitch, and yaw attitude and rate inputs.

Fig. 12: Black Knight Transformer aircraft in hover flight.

Also note that the control systems tested here were designed for slow response typical to a cargo aircraft. There is significant remaining control margin that can be taken advantage of to provide a faster response. Improvements will be made to the control system based on the flight test data and will be tested in the near future.

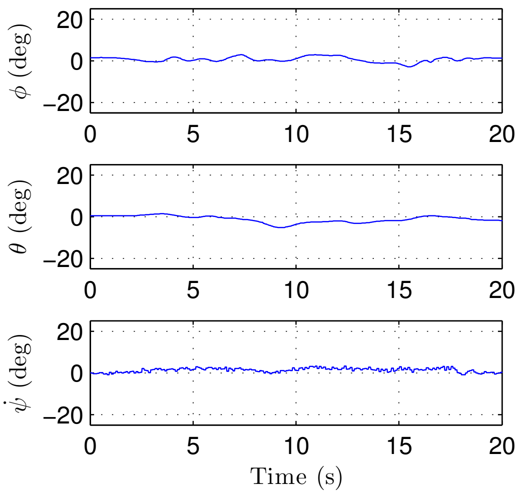

Fig. 13: Aircraft attitude data collected from a hover flight.

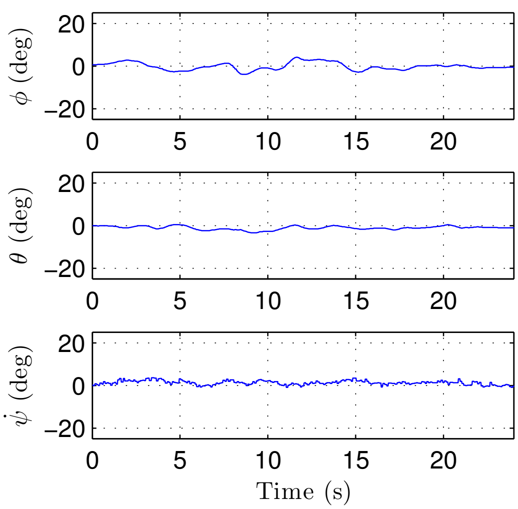

Fig. 14: Aircraft attitude data collected from a different hover flight.

CONCLUSION

The modeling, simulation, and control system design of small scale multicopter aircraft is well understood, but new challenges are introduced when the multicopter is designed at a large scale with gas powered engines. Many of the same modeling techniques can be used; however, several of the assumptions typically made are no longer valid. The response time of a gas powered reciprocating engine is considerably longer than that of an electric motor. The differential-torque yaw method used on small multicopters does not scale well with aircraft size so that a propeller tilting method must be used. Additionally, provisions must be made to allow safe control of the aircraft if an engine fails. The resulting aircraft and control system described in this paper addresses these challenges.

The aircraft control system architecture, which consists of a central flight control computer, sensors, and a network of engine control units and actuator control units, provides a robust platform for control system implementation and data collection. It is also adaptable for integration with higher level flight control units. For instance, the Office of Naval Research's (ONR) Autonomous Aerial Cargo Utility System (AACUS), seeks to develop a platform agnostic helicopter flight control system that would be ideal for integration with the Black Knight Transformer, producing a fully autonomous solution for military missions (Ref. 8).

The successful flight test of the aircraft has provided empirical data to verify the models and simulations developed. The aircraft demonstrated stable and controllable flight and a significant lifting capability. This provides a basis for further control system development and improvement. Continued flight testing will be performed in the near future.

The development of the Black Knight Transformer has been a long and difficult process. We have accomplished a significant amount of work with a small amount of funding and years of hard work and persistance. The result is an aircraft that is novel and has advantages in simplicity, cost, and compactness. It benefits from many of the same advantages that have made the multicopter design so popular for small unmanned aircraft and it offers new capabilities for future manned and unmanned vertical lift missions.

Fig. 15: The Black Knight Transformer technology demonstrator prototype during desert flight testing.

ACKNOWLEDGMENTS

Acknowledgement must be made to Mr. Donald Shaw, the inventor and chief designer of the Black Knight Transformer design. Acknowledgement is also made to the staff and in particular to Dr. Gary Gilbert and Mr. Michael Beebe at the U.S. Army Telemedicine and Advanced Technology Research Center (TATRC) who managed and supported the Black Knight Transformer development program.

REFERENCES

[1]Pounds, P., Mahony, R., and Corke, P., "Modelling and Control of a Large Quadrotor Robot," *Control Engineering Practice*, Vol. 18, 2010.

[2]Hoffman, G., Huang, H., Waslander, S., and Tomlin, C., "Quadrotor Helicopter Flight Dynamics and Control: Theory and Experiment," *AIAA Guidance, Navigation, and Control Conference and Exhibit*, 2007.

[3]Michael, N., Mellinger, D., Lindsey, Q., and Kumar, V., "The GRASP Multiple Micro-UAV Testbed," *Robotics & Automation Magazine, IEEE*, Vol. 17, 2007.

[4]Spakovszky, Z. S., *Thermodynamics and Propulsion Unified*, Massachusetts Institute of Technology, 2008.

[5]Prouty, R. W., *Helicopter Performance, Stability, and Control*, Krieger Publishing Company, 1986.

[6]Yechout, T. R., *Introduction to Aircraft Flight Mechanics*, AIAA Education Series, 2003.

[7]"ADS-33E Aeronautical Design Standard Performance Specification: Handling Qualities Requirements for Military Rotorcraft," 2000.

[8]Warwick, G., "ONR On Track to Demo Autonomous Cargo Resupply," *Aviation Week and Space Technology*, 2013.